

# Quantitative Phase Analysis for Carbide Characterization in Steel Using Automated Electron Diffraction

Stef Smeets,\* Jonas Ångström, and Claes-Olof A. Olsson

Carbides are critical to many different properties in a steel. In this paper, the quantification of a carbide powder extracted from a stainless steel analyzed with profile refinement of X-ray powder diffraction patterns, is compared to a novel technique for automated electron diffraction pattern collection with a transmission electron microscope. The automated analysis has the advantage of collecting patterns from individual particles, hence avoiding issues such as overlapping reflections in powder diffractograms. Electron diffraction patterns with satisfactory quality are selected through a deep convoluted neural network and matched to a library of pre-calculated diffraction patterns, corresponding to a set of selected carbide crystal structures. The quantitative results from the automated particle analysis are in good agreement with the phases identified by powder profile refinement.

carbon compounds have different mechanical properties. By controlling the carbide size and type, it is possible to tailor the mechanical response of the material. The different carbides also have varying contents of chromium, and will thus contribute differently to chromium depletion and consequently to the corrosion resistance of the material.

When modeling carbides, many properties can still be understood by considering hard particles in a softer steel matrix. These particles may serve, for example, as pinning sites for dislocation loops or contributors to creep strength. Following the increasing computational power available, more advanced models now include hardness, magnetic response, and other properties.<sup>[2–4]</sup> A more detailed knowledge

## 1. Introduction

By definition, steel is an alloy of iron and carbon. A big part of the knowledge behind making a good steel, is keeping track of the interaction between these two elements. For more complex alloys, the interaction between carbon and other metallic elements is even more important. Today, most stainless steels are designed to contain less than 0.030 wt% of carbon. Still, carbon has a critical influence on macro properties such as strength, ductility, corrosion resistance, etc. To study the relationship between the carbon and the performance of a steel, it has been found practical to separate the carbon particle distribution into size and chemical composition.

Carbide size distributions determine how fast the particles grow and dissolve. As to what concerns carbide type, different compositions and structures have been reported. The carbide precipitation sequence in stainless steel has been described as Matrix  $\rightarrow$   $M_3C$   $\rightarrow$   $M_7C_3$   $\rightarrow$   $M_{23}C_6$   $\rightarrow$   $M_6C$  with an alternative route Matrix  $\rightarrow$   $M_2C$   $\rightarrow$   $M_{23}C_6$   $\rightarrow$   $M_6C$ , or direct formation of  $MC$ .<sup>[1]</sup> Here, M represents any metal ion, in this context most frequently: iron, chromium or molybdenum. These different

on the actual carbide distribution obtained using X-ray diffraction and high resolution electron microscopy is required to obtain such models. X-ray powder diffraction (PXRD) is a technique, more than a century old, which is very powerful for phase identification and quantification of bulk chemical substances. Quantitative phase analysis (QPA) breaks down the relative abundances of several phases present in a bulk material, and is typically the domain of PXRD. QPA is normally performed using profile refinement of powder diffraction data,<sup>[5]</sup> commonly referred to as Rietveld QPA (RQPA), a technique developed some 30 years ago for X-ray,<sup>[6]</sup> and neutron powder diffraction.<sup>[7]</sup> The accuracy of the method has been well established via large interlaboratory studies.<sup>[8–10]</sup> However, there are several problems associated with RQPA. First, the returned quantities are relative abundances. Secondly, RQPA is limited to well-defined crystalline species, which means that the non-crystalline (amorphous) species that are difficult to quantify are typically ignored. Additionally, there are several characteristics inherent to the material that can affect the RQPA, such as preferred orientation and reflection overlaps from materials with low crystal symmetry and/or large lattice parameters. The difficulty in dealing with the latter increases with the number of phases in a polycrystalline material; the issue is further complicated if these phases have similar lattice parameters, as is the case for many carbides.

In recent years, PXRD has been complemented by alternatives with a high lateral resolution, for example, electron backscatter diffraction. Still, PXRD has the advantage of a very high resolution in the diffractogram, which makes it possible to resolve even minute differences in lattice parameters. For residual stress measurements, it is common practice to work

Dr. S. Smeets, Dr. J. Ångström  
Department of Materials and Environmental Chemistry  
Stockholm University  
SE-114 17 Stockholm, Sweden  
E-mail: stef.smeets@gmail.com

Dr. C.-O. A. Olsson  
Sandvik Materials Technology  
SE-811 81 Sandviken, Sweden

DOI: 10.1002/srin.201800300

with minute peak shifts, corresponding to femtometer displacements.

When studying a bulk metal, the detection limit for secondary phases is normally on a percentage level. Lower phase fractions can be accessed by dissolving the metal matrix and studying the residue isolate. This method is also quantitative, since it is possible to weigh the sample and the residue before and after the dissolution process. The phase isolation process is straightforward for electrically insulating particles, and somewhat more cumbersome for intermetallic phases. The phase isolation process was subject to extensive studies in the 1960s. It is still a viable tool for quantitative bulk estimates and it was recently revisited by Lu et al.<sup>[11]</sup>

Individual carbides can be analyzed in the transmission electron microscope (TEM), but for practical reasons, the number of accessible particles will be limited. This study explores the use of serial electron (SerialED),<sup>[12]</sup> as an alternative method to study the phase fraction of polycrystalline carbides in a TEM, with the hope that it can also provide some additional information to RQPA. In a SerialED experiment, diffraction data are collected from a large number of individual nano- or micro-sized crystals. This is done on a state-of-the-art TEM with the possibility for computer control. The sample stage is translated over a large area and crystals are detected in imaging mode using image recognition techniques. Once some crystals have been located, the electron beam is focused on each of the crystals so that diffraction data can be collected, see **Figure 1**. The method is fully automated, and by combining diffraction data from a large number of crystals, it is possible to obtain quantitative information. As the SerialED data are collected crystal-by-crystal, some of the problems inherent to RQPA, for example, reflection overlaps, are avoided. QPA using SerialED

relies on the ability to match a diffraction pattern to a library of pre-calculated simulated patterns of the expected phases.

In this paper, the automated TEM approach is introduced. It gives access to diffractograms from individual particles, and hence an identification with no or very limited overlaps. This automated identification procedure was found to correlate well with conventional powder profile refinement on an isolate of carbide particles, obtained by electrochemical dissolution of the metal matrix.

## 2. Experimental Section

### 2.1. Material

The carbides were taken from a martensitic stainless steel with nominal composition 0.38C, 0.4Si, 0.6Mn, 13.5Cr, and 1.0Mo. Phase isolates were obtained by an electrolytic process, where the metal matrix was dissolved under potential in an acidic electrolyte. The steel samples were weighed before and after the dissolution. The electrolyte was filtered through an “ad hoc” holder from Sartorius Biotech, and the carbides were collected on the filter paper. To obtain the weight of the carbide deposit, the paper was weighed before and after putting carbides on it. Before each weighing, the filter paper was dried for 60 min at 60 °C. The remaining solid substance consisted exclusively of carbides; their weight fraction was estimated to be 2.9 wt%.

The selectivity of the phase isolation process was checked by studying long term samples where all carbon should be present as carbides. For this type of experiment, a good match was found between the carbon content taken from the heat composition,

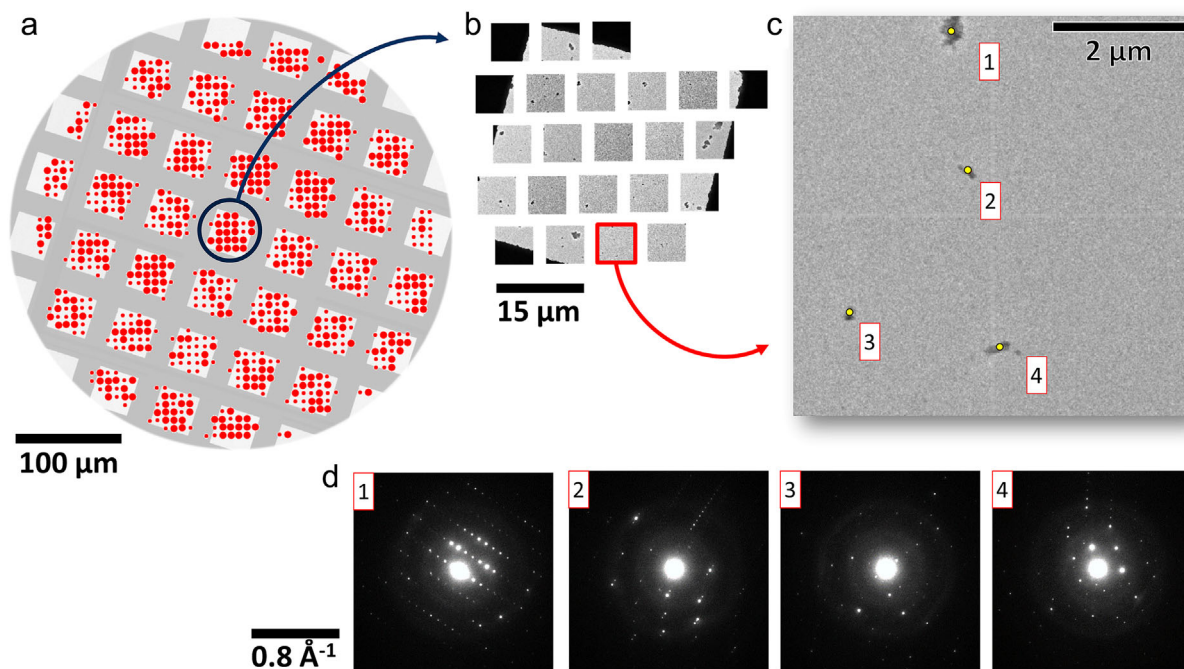


**Figure 1.** a) Low magnification overview of the area on the sample grid where ED data are collected. Each spot corresponds to a position of the sample stage, and an image is taken at each position. The larger red spots indicate images in which crystals have been detected. b) Enlarged view of some of the images. c) Example image where four crystals have been detected, and d) their corresponding diffraction patterns.

**Table 2.** Phase parameters and composition for the constituting carbides.

| Phase | Name              | Space Group  | <i>a</i> (Å) | <i>b</i> (Å) | <i>c</i> (Å) | Comp. (%) |
|-------|-------------------|--------------|--------------|--------------|--------------|-----------|
| 1     | $M_{23}C_6$       | $Fm\bar{3}m$ | 10.62        | <i>a</i>     | <i>a</i>     | 84.5      |
| 2     | $Cr_7C_3$ (hex)   | $P6_3mc$     | 13.77        | <i>a</i>     | 4.88         | 3.1       |
| 3     | $Cr_7C_3$ (ortho) | $Pnma$       | 4.39         | 7.08         | 14.16        | 12.4      |

determined using combustion analysis, and the gravimetric fraction of the isolate. Hence, it appears reasonable to assume that there is low or no preferential loss of carbides during the isolation process. In addition, the filter papers can be checked in an SEM to get a rough quantification and verify that no unexpected contaminants are present in the isolate.

## 2.2. X-Ray Diffraction

The PXRD experiments were performed using a Bruker D8 Advance diffractometer, equipped with a 5-axis Eulerian cradle, a  $CoK\alpha$  ( $\lambda = 1.7890 \text{ \AA}$ ) X-ray source and a LynxEye XE silicon strip detector. The instrument was operated in a focusing Bragg-Brentano mode and the carbides were spun during recording of the diffractogram. The quantification using profile refinement was performed using the Bruker Topas 5.0 software.<sup>[13]</sup>

## 2.3. Transmission Electron Microscopy

Samples were prepared by dispersing the carbide powder in ethanol, followed by a treatment in ultrasound for 5 minutes. Three droplets were transferred to a copper grid with continuous carbon film (CF400-Cu-UL from Electron Microscopy Sciences). After each drop, excess liquid was removed, after which the ethanol was allowed to evaporate. SerialED data were collected on a JEOL JEM-2100-LaB6 at 200 kV equipped with a  $512 \times 512$  Timepix hybrid pixel detector ( $55 \times 55 \mu\text{m}$  pixel size, QTPX-262k, Amsterdam Scientific Instruments) using the approach described in ref. <sup>[12]</sup>. Data were collected using the “ad hoc” software Instamatic.<sup>[14]</sup> Data collection was performed using a small condenser aperture ( $50 \mu\text{m}$ ), spot number 4 (small spot size), a diffraction camera length of 250 mm (giving a maximum resolution  $d_{\text{min}} \approx 1.0 \text{ \AA}$ ), and exposure times of 0.1 s for diffraction patterns and 0.5 s for images. Parallel illumination was used in imaging mode, and the electron beam was focused

using the condenser lens (CL1) in diffraction mode to give an effective probe diameter of approximately 400 nm. The diffraction patterns were focused to give sharp spots using the intermediate lens (IL1). Two grids were prepared, and five data sets were collected covering a total area of approximately  $0.46 \text{ mm}^2$ . A summary of the experimental parameters is given in Table 1.

## 3. Results and Discussion

### 3.1. X-Ray Powder Diffraction

Quantification of X-ray powder diffractograms by refinement is a delicate process. There are many parameters that influence the shape and intensities of PXRD peaks. It is imperative that as much information of the sample as possible is collected prior to the evaluation, and that as few parameters as possible are left free in the final fitting process. The presented fit model has been tested on more than 50 diffractograms from isolates, collected after heat treatments to different times and temperatures. The overall partitioning between different carbides was found to be in accordance with general concepts on carbide formation and structure evolution.

Carbide structures were selected by going through a series of entries in the inorganic crystal structure database (ICSD).<sup>[15]</sup> Especially for the  $M_{23}C_6$  carbides, it appears that the balance between iron and chromium is important to achieve a good match. It is also important to get good profile fits throughout an entire data set. In this case, more than 50 isolates obtained from steels heat treated at different times and temperatures were used to discriminate between a set of structures. To obtain a stable model for carbide evolution, it is also important to use the lowest number of compounds that still gives a reasonable fit quality. This procedure resulted in the selection of three carbides from the ICSD:  $Cr_7C_3$  hexagonal (ICSD No. 52289),<sup>[16]</sup>  $Cr_7C_3$  orthorhombic (ICSD No. 181713),<sup>[17]</sup> and  $M_{23}C_6$  (ICSD No. 62670).<sup>[18]</sup> The details of these phases are given in Table 2. By spinning the sample during the analysis, it was possible to avoid applying corrections for preferential orientations, with the exception of the (1 1 1) peak in the  $M_{23}C_6$  carbides where a March-Dollase correction was introduced to obtain a satisfactory fit.

Other parameters in the refinement structure model were set up with a background approximated with a second order Chebyshev polynomial together with a  $1/x$  component. Instrument parameters such as goniometer radii, axial convolutions as well as source and detector geometries were set to

**Table 1.** Summary of the SerialED experiments.

| Exp. | Area [ $\mu\text{m}^2$ ] | Positions probed | Images | Patterns | Time [mins] | Patterns per hour |
|------|--------------------------|------------------|--------|----------|-------------|-------------------|
| 1a   | $400 \times 400$         | 1941             | 861    | 1559     | 77          | 1214              |
| 1b   | $300 \times 300$         | 1060             | 535    | 753      | 45          | 1004              |
| 2a   | $300 \times 300$         | 1060             | 467    | 144      | 40          | 216               |
| 2b   | $300 \times 300$         | 1060             | 473    | 464      | 44          | 632               |
| 2c   | $400 \times 400$         | 1941             | 836    | 1019     | 81          | 754               |

the real values. The  $\text{CoK}_\alpha$  radiation was approximated with a seven-line model as provided in Topas 5. To allow for small errors in height positioning, the sample displacement was left free. The peak was calculated using a first principles peak shape, which allows for interpreting peak broadening in terms of crystal size or strain. For the carbide powder in this study, the peak broadening was accounted for by fitting a Lorentzian crystal size contribution, which could give some information on the size distribution of the carbides after compensation for the instrumental broadening. The atom coordinates and the occupancy used were taken directly from the ICSD database and kept constant throughout the fit series. The equivalent isotropic temperature factors were also set to unity for all fits. Thus, the free parameters necessary for a satisfactory fit were 3 background parameters, z-displacement, lattice, scale and peak broadening parameters for all phases as well as one preferential orientation parameter for the  $\text{M}_{23}\text{C}_6$  carbide.

One sample from the larger data set was selected for automated TEM analysis. **Figure 2** shows a diffractogram together with the resulting automated fit envelope as well as the partial curves for the three carbides. By studying the partial fit curves from the different carbides, it can be seen that all three components are necessary. Additional peaks in the diffractogram are oxides that originate from oxidizing water during the first seconds of the experiments. The water is present from the >30% hydrochloric acid used to prepare the electrolyte, which results in a brief initial water splitting at the start of the electrolytic dissolution process. The respective phase parameters obtained for the fit, see Table 2, were then used as base input for identification and data processing in the automated TEM method.

### 3.2. Automated Transmission Electron Microscopy

Opposed to PXRD, which is a bulk method, a TEM makes it possible to probe individual crystallites, but doing so manually is very time consuming. The SerialED method that we have developed makes it possible to probe an arbitrarily large number of individual crystallites automatically.<sup>[12]</sup> The phase of the material can be deduced by comparing the diffraction pattern with a library of pre-calculated patterns.

Data were acquired on the same phase isolate used for the PXRD study. Five different data collections were carried out in total, using two different grids, with each data collection covering a different area of the grid. In total, diffraction data on almost 4000 crystals were collected at a rate of approximately 800 crystals per hour. In a previous study, rates of up to 4000 crystals per hour for grids with a high density of crystals have been achieved,<sup>[12]</sup> but in this case the distribution of crystals is rather sparse. On the other hand, this means that the crystals are well isolated, which is an advantage for data collection.

Standard SerialED data pre-processing (i.e., finding the center of the diffraction pattern, background subtraction, peak identification) and orientation finding was performed as described previously<sup>[12]</sup> using the code available from ref. <sup>[19]</sup>. The phase matching was performed using a direct orientation finding algorithm with the provided unit cells (Table 2). For this procedure, a library of all crystallographically unique orientations was generated (with polar coordinates  $\alpha$ ,  $\beta$  defining the zone-axis, and  $\gamma$  defining the in-plane rotation, so that all orientations are spaced roughly  $1.7^\circ$  apart). The corresponding calculated diffraction patterns are then compared one-by-one with each observed pattern. For any given measured pattern, the

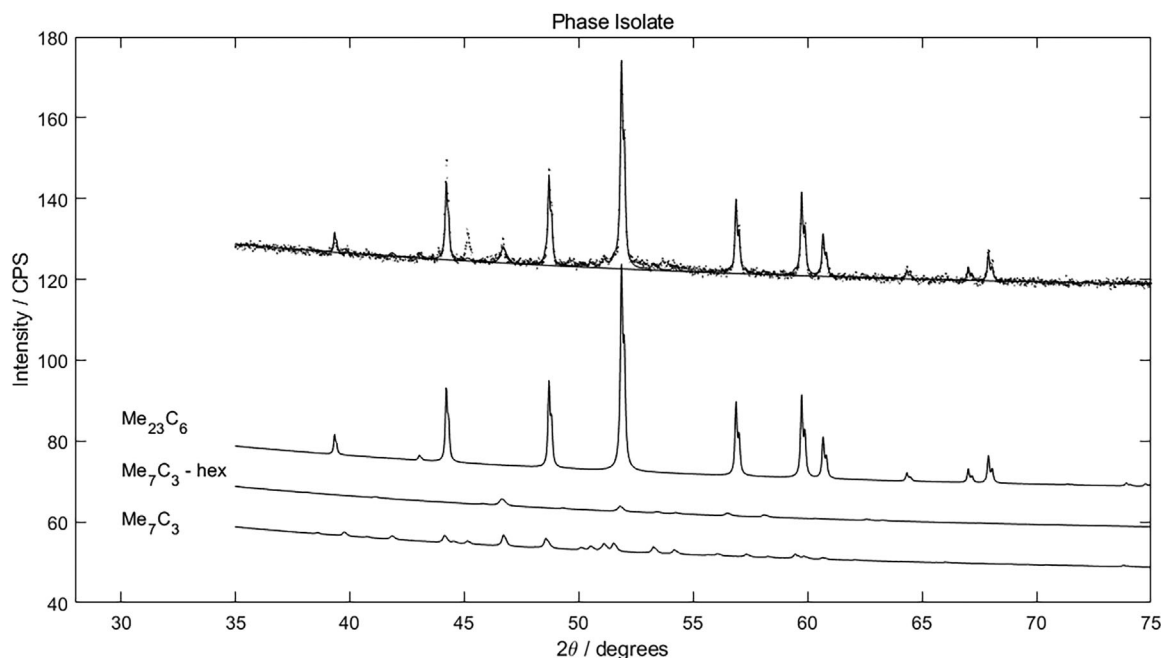


**Figure 2.** Powder diffractogram with automated profile fits. The upper part contains the acquired diffractogram (dots) with the fit envelope (solid line). Fit curves for the included partial components are shown below. A narrow region around  $50^\circ$  is shown. For the fits, a region from  $30$  to  $120^\circ$  was used.

corresponding calculated pattern with the best match (as determined by an indexing *score*) is assumed to be correct. This is followed by a least-squares optimization of the orientation against the same metric. For additional details, see Smeets et al.<sup>[12]</sup> To perform QPA, the procedure is repeated for each given unit cell, where the best match determines both the orientation and the crystalline phase of the crystal.

### 3.2.1. Quantitative Phase Analysis

One of the properties that makes QPA with SerialED data difficult is that data with a widely varying quality are collected. Frequently, these belong to agglomerates, which can give powder rings or cluttered diffraction patterns, crystals that are too thick or of poor quality (e.g., low crystallinity), or false positives (e.g., from the copper grid). Perhaps the poor crystallinity of some crystals can be attributed to the dissolution process. It is also known that  $M_7C_3$  often gives rise to streaking in the diffraction pattern which has also been observed in the data presented here. The orientation finding method works best with crystals that produce sharp and well-defined spots, and perhaps at somewhat reduced precision in the case of the streaking.

There were concerns that some of the low quality diffraction patterns would be wrongly indexed for the reasons stated above. Thus, the indexing score is used as a qualifier to assess whether a diffraction pattern is suitable for calculating a representative phase fraction. This is done by setting a threshold  $T$ , where solutions with a score equal or lower than  $T$  are discarded ( $score > T$ ). Initially, the method was tested using the 1559 patterns obtained from experiment 1a. First, all solutions with a score of 0 are removed ( $T = 0$ ), leaving 1081 patterns with a phase fraction of 44.1%, 6.5%, and 49.4% for phases 1, 2, and 3, respectively. Then, the threshold was increased to reduce the contribution of low quality patterns to the phase quantification. The idea is that a higher value for  $T$  results in the acceptance of a lower number of patterns, but that these may be of more reliable quality. With  $T = 100$ , 642 patterns are discarded, leaving 439 with a corresponding phase fraction of 38.3%, 6.2%, and 55.6% for phases 1, 2, and 3, respectively. The main difference appears to be in the fraction of phases 1 and 3. When  $T$  is increased further, the difference is smaller. A similar trend is observed for experiment 1b, but 2a, 2b, and 2c are more consistent when  $T$  is varied. A summary of the QPA using SerialED for all samples is given in Table 3. Despite this, the phase fractions are fairly consistent across all experiments using  $T = 100$  or higher, but it was still unclear whether this method produced reliable results. In addition, the choice of  $T$  is subjective, possibly introducing bias that is difficult to avoid.

### 3.2.2. Machine Learning

To make optimal use of the orientation finding and phase identification algorithm, the QPA should be performed using on the good diffraction patterns only. It was clear that the indexing score is simply not a good metric for determining whether a diffraction pattern is of satisfactory quality or not, because there may be several reasons why a pattern cannot be indexed. The

**Table 3.** Phase analysis results from the SerialED data using different selection criteria.

| Exp.         | Method <sup>a)</sup> | $N_{selected}$ | $N_{phase1}$ | $N_{phase2}$ | $N_{phase3}$ |
|--------------|----------------------|----------------|--------------|--------------|--------------|
| 1a (1559)    | $T = 0$              | 1081           | 477 (44.1%)  | 70 (6.5%)    | 534 (49.4%)  |
|              | $T = 100$            | 439            | 168 (38.3%)  | 27 (6.2%)    | 244 (55.6%)  |
|              | $T = 200$            | 301            | 111 (36.9%)  | 22 (7.3%)    | 168 (55.8%)  |
|              | CNN                  | 253            | 78 (30.8%)   | 10 (4.0%)    | 165 (65.2%)  |
| 1b (753)     | $T = 0$              | 657            | 284 (43.2%)  | 54 (8.2%)    | 319 (48.6%)  |
|              | $T = 100$            | 261            | 90 (34.5%)   | 25 (9.6%)    | 146 (55.9%)  |
|              | $T = 200$            | 165            | 57 (34.5%)   | 17 (10.3%)   | 91 (55.2%)   |
|              | CNN                  | 145            | 54 (37.2%)   | 15 (10.3%)   | 76 (52.4%)   |
| 2a (144)     | $T = 0$              | 118            | 43 (36.4%)   | 12 (10.2%)   | 63 (53.4%)   |
|              | $T = 100$            | 95             | 33 (34.7%)   | 12 (12.6%)   | 50 (52.6%)   |
|              | $T = 200$            | 83             | 30 (36.1%)   | 11 (13.3%)   | 42 (50.6%)   |
|              | CNN                  | 49             | 17 (34.7%)   | 5 (10.2%)    | 27 (55.1%)   |
| 2b (464)     | $T = 0$              | 402            | 140 (34.8%)  | 26 (6.5%)    | 236 (58.7%)  |
|              | $T = 100$            | 235            | 77 (32.8%)   | 18 (7.7%)    | 140 (59.6%)  |
|              | $T = 200$            | 168            | 51 (30.4%)   | 14 (8.3%)    | 103 (61.3%)  |
|              | CNN                  | 159            | 50 (31.4%)   | 9 (5.7%)     | 100 (62.9%)  |
| 2c (1019)    | $T = 0$              | 832            | 308 (37.0%)  | 44 (5.3%)    | 480 (57.7%)  |
|              | $T = 100$            | 500            | 182 (36.4%)  | 29 (5.8%)    | 289 (57.8%)  |
|              | $T = 200$            | 324            | 114 (35.2%)  | 18 (5.6%)    | 192 (59.3%)  |
|              | CNN                  | 352            | 127 (36.1%)  | 22 (6.2%)    | 203 (57.7%)  |
| Total (3939) | $T = 0$              | 3090           | 1252 (40.5%) | 206 (6.7%)   | 1632 (52.8%) |
|              | $T = 100$            | 1530           | 550 (35.9%)  | 111 (7.3%)   | 869 (56.8%)  |
|              | $T = 200$            | 1041           | 363 (34.9%)  | 82 (7.9%)    | 596 (57.2%)  |
|              | CNN                  | 958            | 323 (33.7%)  | 61 (6.4%)    | 571 (59.6%)  |

<sup>a)</sup> The method used to select the  $N_{selected}$  patterns for phase quantification.

intension was to separate the identification of good quality diffraction patterns from the orientation finding algorithm. For this purpose, a method to distinguish between “good” and “bad” diffraction patterns using machine learning was developed. A deep convoluted neural network (CNN) was trained on approximately 78 000 patterns from many different experiments where 57% were labeled “good” and 43% were labeled “bad”. More details will be provided in a future paper, but here follows a brief description.

Before being input into the CNN, the diffractogram is centered so the central beam is in the middle of the image, the values of the pixels are normalized to lie between 0.0 and 1.0 and finally the image is resized to 150 by 150 pixels. The network consists of five convolutional layers followed by two dense layers and an output layer. The convolutional layers automatically learns features in the image, starting by  $3 \times 3$  pixel features in the first one, followed by larger and larger features in the following layers, built from the features found in the preceding layer. The features found in the final convolutional layer are fed into the dense layers. These produce a value between 0.0 and 1.0 in the output layer depending on the combination of features found in the final convolutional layer. Ideally a “good” diffraction pattern should yield 1.0 and a “bad” one 0.0, but any value above

0.5 is classified as “good”. From the training, testing, and validation, the CNN was expected to be about 93% accurate.

For this study, 958 out of all 3939 diffraction patterns (24.3%) passed the 0.5 threshold. A possible explanation for the low number of particles with acceptable pattern quality can be attributed to the presence of streaking in many of the patterns, considering that the CNN was trained to accept spot patterns. A selection of diffraction patterns and the predictions are shown in **Figure 3**. The other diffraction patterns were eliminated from the list. The orientation finding procedure as described above was repeated with the reduced list. The resulting phase fractions, which can be found in Table 3, are consistent over the 5 experiments. It was found that over the whole data set, with 958

diffraction patterns, 323 (33.7%) belong to phase 1, 61 (6.4%) to phase 2, and 571 (59.6%) to phase 3. Based on these data, the error on the phase composition from SerialED data is estimated to be in the order of  $\pm 5.0\%$ . Importantly, the numbers are consistent with those obtained using  $T = 100$  or  $T = 200$ . This indicates that the small subset of patterns selected by the CNN is representative for the larger data set.

### 3.2.3. Comparison with PXRD

The numbers obtained using SerialED differ from those found using the RQPA method. The main reason is that the number of

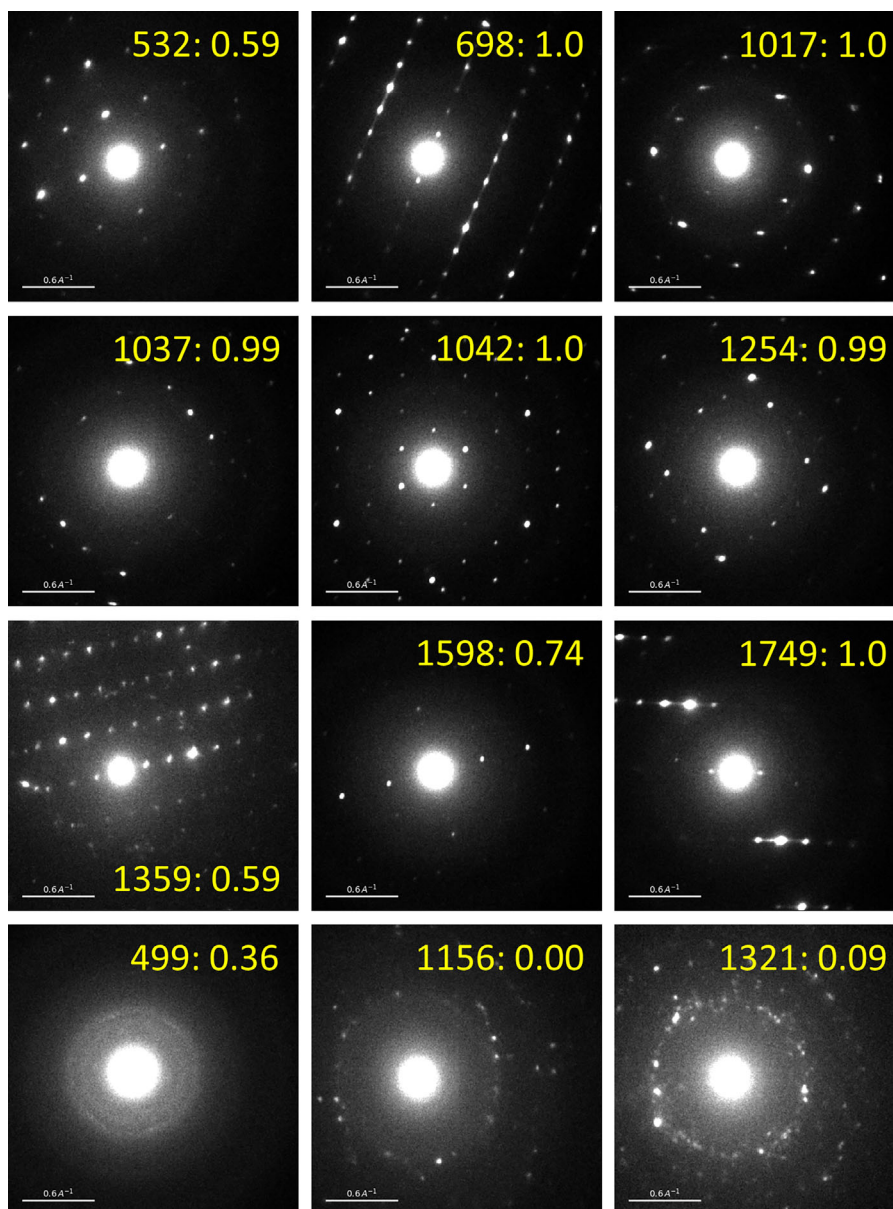


**Figure 3.** Selection of satisfactory (top three rows) and less satisfactory (bottom row) diffraction patterns as predicted by the neural network from experiment 2c. Sequence numbers and prediction scores are given for each pattern individually.

crystals belonging to a phase are counted, rather than the relative weight percentages. This information is complementary to what is obtained from PXRD data through RQPA. Another point is that not all crystals are used for the phase quantification, only those with well-defined spot patterns. One of the reasons is that only the crystal lattice parameters and corresponding space group are used to match a diffraction pattern to its corresponding phase, and this can affect the accuracy of the method. In the future, an option may be to use the relative reflection intensities that can be calculated from the known crystal structure. This would provide additional constraints for the phase matching, as is standard practice for orientation mapping.<sup>[20,21]</sup>

Phase matching using PXRD data depends on the availability of large databases, such as the ICSD,<sup>[15]</sup> that have been established for quickly matching a powder pattern to a large number of known phases. Likewise, phase matching using SerialED also depends on the fact that the correct phases are known beforehand. In this study, the phases were selected based on the information obtained from the PXRD data. An advantage of using a TEM, on the other hand, is that the structure of any unknown crystalline phase can be determined by collecting single-crystal electron diffraction (SCED) data on an isolated crystal.<sup>[22]</sup> One downside with the SerialED method is the absence of a residual curve, which is sometimes used as a fit quality measure in the RQPA process. Any unknown particles will show up as not indexed. One example in this paper is the diffraction peak near 45°, which is attributed to an oxide, but not included in the phases used for RQPA or quantitative electron diffraction.

## Conclusions

This work demonstrated automated carbide characterization using PXRD and TEM techniques that allow for the identification of a large number of individual carbides. The SerialED technique makes it possible to resolve individual carbides in the material. Based on these findings, it can be concluded that it is possible in principle to perform QPA using SerialED data. However, the phase matching, that is, used to classify the diffraction data is largely dependent on their quality; the diffraction pattern should have sharp spots (no diffuse scattering), reasonably high resolution, and contain no alien spots (i.e., from a second crystal). For this reason, a deeply convoluted neural network was used to predict which diffraction data are of sufficient quality. Performing the analysis on the reduced data confirmed that the phase fractions that are consistent across the 5 different experiments. The phase fractions from the automated TEM procedure complements the compositions obtained from quantification of PXRD data on phase isolates, considering that the first measures the number of particles and the latter weight percent. The SerialED method also lends itself for combination with other methods, such as energy-dispersive X-ray spectroscopy (EDS) and particle size analyses, and therefore opens up new possibilities for understanding and controlling carbide formation in steel through repeated experiments.

## Acknowledgements

Per Lindström, Sandvik R&D, was gratefully acknowledged for making the phase isolates. The anonymous reviewers were thanked for critically reading the manuscript and suggesting improvements. S. S. thanked the Swiss National Science Foundation for financial support (project numbers: 165282, 177761). The electron microscopy work was supported by the Knut and Alice Wallenberg Foundation through the project grant 3DEM-NATUR.

## Conflict of Interest

The authors declare no conflict of interest.

## Keywords

carbide, powder profile refinement, stainless steel, transmission electron microscopy, x-ray diffraction

Received: June 11, 2018  
Published online: September 6, 2018

- [1] G.-J. Cai, *PhD thesis*, Chalmers Institute of Technology, SE-412 96 Gothenburg, Sweden, **1994**.
- [2] S. Ma, J. Xing, Y. He, Y. Li, Z. Huang, G. Liu, Q. Geng, *Mater. Chem. Phys.* **2015**, *161*, 65.
- [3] Y. Liu, Y. Jiang, J. Xing, R. Zhou, J. Feng, *J. Alloys Compd.* **2015**, *648*, 874.
- [4] C. M. Fang, M. A. van Huis, M. Sluiter, *Acta Mater.* **2016**, *103*, 273.
- [5] B. O. Loopstra, H. M. Rietveld, *Acta Crystallogr. B* **1969**, *25*, 787.
- [6] D. L. Bish, S. A. Howard, *J. Appl. Crystallogr.* **1988**, *21*, 86.
- [7] B. O'Connor, M. Raven, *Powder Diffr.* **1988**, *3*, 2.
- [8] I. C. Madsen, N. V. Y. Scarlett, L. M. D. Cranswick, T. Lwin, *J. Appl. Crystallogr.* **2001**, *34*, 409.
- [9] L. León-Reina, A. G. De la Torre, J. M. Porras-Vázquez, M. Cruz, L. M. Ordonez, X. Alcobé, F. Gispert-Guirado, A. Larrañaga-Varga, M. Paul, T. Fuellmann, R. Schmidt, M. A. G. Aranda, *J. Appl. Crystallogr.* **2009**, *42*, 906.
- [10] T. Fawcett, F. Needham, J. Faber, C. Crowder, *Powder Diffr.* **2010**, *25*, 60.
- [11] J. Lu, J. B. Wiskel, O. Omotoso, H. Henein, D. G. Ivey, *Metall. Mater. Trans. A* **2011**, *42*, 1767.
- [12] S. Smeets, X. Zou, W. Wan, *J. Appl. Crystallogr.* **2018**, *51*, DOI: 10.1107/S1600576718009500.
- [13] A. A. Coelho, *J. Appl. Crystallogr.* **2018**, *51*, 210.
- [14] S. Smeets, B. Wang, M. O. Cichocka, J. Angström, W. Wan, *Instamatic 0.4*, Zenodo, **2017**, DOI: 10.5281/zenodo.1090389.
- [15] A. Belsky, M. Hellenbrandt, V. L. Karen, P. Luksch, *Acta Crystallogr. B* **2002**, *58*, 364.
- [16] A. Westgren, *Jernkontorets Annaler* **1935**, *119*, 231.
- [17] Y. Li, Y. Gao, B. Xiao, T. Min, Y. Yang, S. Ma, D. Yi, *J. Alloys Compd.* **2011**, *509*, 5242.
- [18] H. L. Yakel Jr. *Acta Crystallogr. B* **1987**, *43*, 230.
- [19] S. Smeets, *Problematic*, [www.github.com/stefsmets/problematic](http://www.github.com/stefsmets/problematic), **2018**, Accessed: 2018-05-01.
- [20] E. F. Rauch, L. Dupuy, *Arch. Metall. Mater.* **2005**, *50*, 87.
- [21] E. F. Rauch, J. Portillo, S. Nicolopoulos, D. Bultreys, S. Rouvimov, P. Moeck, *Z. Kristallogr. Cryst. Mater.* **2010**, *225*, 103.
- [22] Y. Yun, X. Zou, S. Hovmöller, W. Wan, *IUCrj* **2015**, *2*, 267.